MreC and MreD balance the interaction between the elongasome proteins PBP2 and RodA

Xiaolong Liu[1], Jacob Biboy[2], Waldemar Vollmer[2], Tanneke den Blaauwen[1*]

[1] Bacterial Cell Biology, Swammerdam Institute for Life Science, Faculty of Science, University of Amsterdam, 1098 XH, Amsterdam, The Netherlands.

[2] Centre for Bacterial Cell Biology, Institute for Cell and Molecular Biosciences, Newcastle University, NE2 4AX, Newcastle upon Tyne, United Kingdom.

Correspondence: *T. den Blaauwen, Bacterial Cell Biology and Physiology, Swammerdam Institute for Life Sciences, University of Amsterdam, P.O. Box 94215, 1090 GE Amsterdam, The Netherlands

Running Title: Checks and Balances of Elongasome in *Escherichia coli*

Key words: elongasome, PBP2, RodA, MreBCD, conformation, FRET.

Abstract

Rod-shape of most bacteria is maintained by the elongasome, which mediates the synthesis and insertion of peptidoglycan into the cylindrical part of the cell wall. The elongasome contains several essential proteins, such as RodA, PBP2, and the MreBCD proteins, but how its activities are regulated remains poorly understood. Using *E. coli* as a model system, we investigated the interactions between core elongasome proteins *in vivo*. Our results show that PBP2 and RodA form a complex mediated by their transmembrane and periplasmic parts and independent of their catalytic activity. MreC and MreD also interact directly with PBP2. MreC elicits a chance in the interaction between PBP2 and RodA, which is suppressed by MreD. The cytoplasmic domain of PBP2 is required for this suppression. We hypothesize that the *in vivo* measured PBP2-RodA interaction change induced by MreC corresponds to the conformational change in PBP2 as observed in the MreC-PBP2 crystal structure, which was suggested to be the “on state” of PBP2. Our results indicate that the balance between MreC and MreD determines the activity of PBP2, which could open new strategies for antibiotic drug development.

Importance

The cell envelope of *Escherichia coli* bears the protective and shape-determining peptidoglycan layer sandwiched between the outer and inner membranes. Length growth in bacteria is accomplished by a protein complex termed elongasome. We used Förster Resonance Energy Transfer (FRET) that reports not only on whether proteins interact with each other but also on conformational changes during interactions, to investigate how the

elongasome might be activated. RodA and PBP2 provide the peptidoglycan glycosyltransferase and transpeptidase activities needed to synthesize new peptidolgycan during length growth, respectively, and PBP2 activates RodA. We show that the interactions between MreC and MreD with PBP2-RodA alter the nature of the interaction between PBP2 and RodA and hypothesis that the corresponding conformational change in the PBP2-RodA complex allows switching between the 'on' and 'off' states of the elongasome.

Introduction

Bacterial cells are surrounded by a peptidoglycan layer that maintains their shape and protects them from bursting due to the osmotic pressure. The biosynthesis of peptidoglycan is the target of many antibiotics that are used in clinical therapies for bacterial infections. The spread of antibiotic resistant pathogens calls urgently for the development of novel antibiotics. In depth knowledge on peptidoglycan synthesis will aid in the development of effective screening assays to select cell wall synthesis inhibitors. Peptidoglycan is a mesh-like heteropolymer of glycan chains of Glc*N*Ac-Mur*N*Ac-peptide subunits that are connected by peptide cross-links (1). Peptidoglycan synthesis begins in the cytoplasm with synthesis of UDP-Glc*N*Ac and UDP-Mur*N*Ac-pentapeptide (2). Two following membrane steps, catalyzed by MraY and MurG, assemble the precursor lipid II (3, 4), which is flipped to the periplasmic side of the cytoplasmic membrane by lipid II flippase(s) MurJ and/or FtsW (5–7). Glc*N*Ac-Mur*N*Ac pentapeptide units are polymerized into glycan chains and the peptides are cross-linked to bridge the glycan stands by peptidoglycan synthases to expand the peptidoglycan layer while the

carrier lipid is recycled (8–10). Most rod-shaped bacteria employ two protein complexes, elongasome and divisome, to guide peptidoglycan synthesis during lateral growth and cell division, respectively (11).

In *E. coli*, the divisome contains more than twenty proteins. Assembly of the divisome starts with positioning the FtsZ ring at midcell together with other early divisome proteins, such as FtsA, ZipA, ZapA and FtsEX, to form the early divisome (12–14) Subsequently, the late divisome proteins, FtsK, FtsBLQ, FtsW, PBP3 and FtsN, are recruited (15). These proteins localize to midcell in an interdependent order (15, 16). Among these proteins, FstW, PBP3 and PBP1B provide the peptidoglycan synthesis activity during septum synthesis (10, 17, 18). PBP1B has both glycosyltransferase (GTase) and transpeptidase (TPase) activity (19), while FtsW and PBP3 (also called FtsI) only have GTase activity and TPase activity, respectively (10). Although the mechanisms of peptidoglycan synthesis regulation is not fully understood, recent studies showed that the cell division proteins have competing effects and either inhibit (FtsQLB complex) or stimulate the activities of FtsW-PBP3-PBP1B (20–22).

Proteins that are known to be part of the elongasome are the cytoplasmic membrane associated actin homologue MreB, the bitopic membrane proteins RodZ, MreC and PBP2, and the integral membrane proteins MreD and RodA (Fig. 1a). MreB polymerizes into short filaments that rotate around the cylindrical part of the cell (23, 24). The rotation of MreB is believed to drive the topography of the insertion of peptidoglycan into the lateral wall (23, 25–27). Bacterial two hybrid analysis showed that MreB interacts with MreC, but not with MreD (28), while RodZ interacts strongly with

itself, MreB and MreC (28, 29) (Fig.1b), and these interactions are essential to maintain bacterial morphology (28, 30–32). RodA and PBP2 form a stable subcomplex (33) and provide GTase and TPase activity, respectively, during cylindrical peptidoglycan synthesis (9, 34, 35). This subcomplex also shows a circumferential motion that is similar to that of MreB. The bifunctional GTase-TPase PBP1A interacts with PBP2 and stimulates its activity (18). Because PBP1A moves independently of the rotation of PBP2 and MreB, it is thought not to be part of the core elongasome (18, 36). However, the function and role of most elongasome proteins are still poorly understood. How peptidoglycan synthesis is activated and regulated during elongation is still the key question. In this study, combining genetics, microscopy and Förster Resonance Energy Transfer (FRET), we investigated the functions of, and interactions between, these core elongasome proteins. The transfer of energy between a donor fluorescent-protein fusion and an acceptor fluorescent-protein fusion (FRET) is very sensitive to distance, which even allows the detection of conformational changes that affect this distance (7). Our results indicate that MreC and MreD modulate the interaction between PBP2 and RodA in oppositely, which likely reflects a mechanism of elongasome activation and regulation.

Results

RodA and PBP2 activities are not essential for their interaction

RodA and PBP2 form a stable peptidoglycan synthesizing subcomplex in the cytoplasmic membrane as detected by FRET (33). To investigate whether this interaction relies on their enzymatic activities, RodA^{R109A} and RodA^{Q207R}

versions, which were predicted to be inactive based on studies on its homologue FtsW, were constructed (Supplementary Fig. 1) (5, 38). As expected, these mutants could not complement the temperature sensitive RodA strain LMC882 at the non-permissive temperature, and the RodA^{Q207R} variant even showed dominant negative effects at the permissive temperature (Fig. 2a). Subsequently, N-terminal mCherry fused versions (33, 34) of the inactive RodA proteins were expressed to test their interaction with mKO-PBP2^{WT} by FRET (Fig. 2b). In our FRET system, the direct fused mCherry-mKO tandem was used as positive control (33). To account for possible interactions between proteins due to crowding in the cytoplasmic membrane, an integral membrane protein unrelated to peptidoglycan synthesis, GlpT[3,34], was fused to mKO, and its interaction with mCh-RodA was detected as negative control. The acceptor FRET efficiency values (Ef_A) of all FRET samples were calculated using our previously published mKO-mCh FRET spectral unmixing method (33) (Supplementary Fig. 2a). An Ef_A value of 31.0 ± 4.0% was observed for the tandem control (Fig. 2b and Table 1), which is comparable to the published data (33). An Ef_A value of 1.1 ± 3.5% was observed for the RodA-GlpT negative control (Fig. 2b and Table 1). FRET experiments with PBP2^{WT} and RodA^{R109A} or RodA^{Q207R} yielded Ef_A values of 12.5 ± 1.9% and 12.7 ± 1.2%, respectively, which are comparable to the Ef_A value of 12.7 ± 1.7% of wild type RodA, indicating an interaction between PBP2^{WT} and all RodA versions (Fig. 2b, Supplementary Fig 2a and Table 1). To determine whether the activity of PBP2 was required for the interaction with RodA, we expressed the inactive variant PBP2^{S330C}, which is not able to bind benzylpencillin (35). PBP2^{S330C} had a strong dominant negative effect

during the complementation in the PBP2 temperature sensitive strain LMC582 (Fig. 2c), while the detected Ef_A value of $PBP2^{S330C}$-$RodA^{WT}$ remained 10.9 ± 0.5%, which was slightly below the Ef_A value of $PBP2^{WT}$-$RodA^{WT}$ (Fig. 2b and Table 1). These results imply that the activities of RodA and PBP2 are not needed for their interaction.

The transmembrane and periplasmic parts of PBP2 contribute to its interaction with RodA

To reveal which part of PBP2 interacts with RodA, two domain swap mutants of PBP2 were constructed. The cytoplasmic N-terminus (NT) and or the N-terminal region with the transmembrane-helix (NT-TMH) of PBP2 were replaced by the corresponding N-terminal stretches of MalF, a bitopic membrane protein that has been previously used in domain swap studies (39–41), to yield ^{MalFNT}PBP2 and ^{MalF37}PBP2, respectively (Fig. 3a). Both versions of PBP2 were able to localize to the membrane but showed dominant negative effects, indicating the essentiality of the replaced parts (Fig. 3b). The replacement of the NT of PBP2 did not change its interaction with RodA, as the detected Ef_A value remained 14.4 ± 1.1%, which was not significantly different compared to that of the interaction between RodA and wild type PBP2 (Fig. 3c, Table 1 and Supplementary Fig. 2b). However, replacement of the TMH of PBP2 significantly reduced the Ef_A value between PBP2 and RodA to 8.2 ± 1.3%, which reflected an apparent distance increase from 8.6 nm to 9.8 nm between the two proteins (42) (Fig. 3c and Table 1). This decrease in distance was not caused by a change in amount of measured fluorescence for the RodA and PBP2 fusions expressed in the cells

(Supplementary Fig. 2b), or due to the shorter transmembrane helix after replacement (Fig. 3a). The average rise per residue in transmembrane helices is 0.15 nm (43), therefore the two amino acid residues shorter helix in ^{MalF37}PBP2 (Fig. 3a) could maximally change the distance between donor and acceptor fluorophores by 0.3 nm. The still considerably higher Ef_A value compared to the negative control indicates that the transmembrane helix alone is not sufficient for the interaction between PBP2 and RodA and that the periplasmic domain of PBP2 is also involved in this interaction (Fig. 3d).

MreC interacts with PBP2 and affects PBP2-RodA interaction

A recent study of PBP2-MreC from *Helicobacter pylori* showed two different structural conformations of PBP2 in the MreC-bound and unbound forms, respectively[43] (Fig. 4 a). The authors proposed that the binding of MreC to the periplasmic hydrophobic zipper of PBP2 induces a conformational change in PBP2 and a switch from an off state into an on state (44). In our FRET system about 1000 copies of the mKO fusion proteins per cell are expressed from a plasmid (45). The ~180 endogenous copies of MreC molecules (46) are not sufficient to activate the majority of the by plasmid expressed mKO-PBP2 molecules. Therefore, we hypothesize that most of the mildly overexpressed PBP2 versions remain in the off state conformation (Fig. 4b, left). We reasoned that the interaction between PBP2 and RodA could be sensitive to possible conformational changes of PBP2, if we would additionally express MreC to balance the molecule numbers of both proteins. To this end we first tested the interaction between a functional mCh-MreC (28) fusion and mKO-PBP2 by FRET measurements. The observed Ef_A value of 5.1 ± 1.2%

199 indicates a direct interaction between PBP2 and MreC (Fig. 4c, table 1 and
200 Supplementary Fig. 3), which is in agreement with the structural study of
201 PBP2-MreC from *Helicobacter pylori* (44).
202
203 We next we employed a three-plasmids-FRET system that expressed MreC
204 from a third plasmid when testing the interaction between PBP2 and RodA
205 (Fig. 4d, Table 2 and Supplementary Fig. 4). A control strain contained an
206 empty plasmid instead of the MreC-expression plasmid. In the presence of the
207 empty plasmid, the calculated Ef_A values for the tandem (positive control) and
208 RodA-GlpT (negative control) were 30.4 ± 1.8% and 2.3 ± 1.3%, respectively
209 (Fig. 4d and Table 2). These Ef_A values remained unchanged in the presence
210 of MreC expressed from the third plasmid (Fig. 4d and Table 2). Interestingly,
211 the Ef_A value for the RodA-PBP2 interaction was significantly reduced to 4.9 ±
212 0.6% in the presence of MreC, compared with the Ef_A of 8.8 ± 1.1% in the
213 presence of empty plasmid (Fig. 4d and Table 2). These results indicate that
214 MreC changes the interaction between PBP2 and RodA, which would be
215 consistent with an conformational change of PBP2 from the off state to the on
216 state proposed from the crystal structures (44) (Fig. 4b, middle).
217
218 **MreD suppresses the MreC-mediated change in the PBP2-RodA**
219 **interaction**
220 During our study, we noticed that overexpression of MreC caused
221 morphological defects of the wild type strain, increasing the diameter of *E. coli*
222 cells (Fig. 4e and Supplementary Fig. 5). Interestingly, the co-expression of
223 MreD together with MreC suppressed these morphological defects and

224 restored the wild type phenotype (Fig. 4e and Supplementary Fig. 5). To
225 further investigate this effect, we aimed to express an N-terminal functional
226 mCherry fusion of MreD (30) which is an integral membrane protein with 6
227 predicted transmembrane helices and both termini localized in the cytoplasm
228 (Supplementary Fig. 6). Consistent with this topology model we readily
229 observed fluorescence signals for N-terminal fused GFP-MreD (30) and mKO-
230 MreD versions, which could not be possible if the N-terminus of MreD would
231 localize in the oxidative periplasm where GFP and mKO do not mature (37).
232 Similarly as for MreC, the overexpression of MreD alone resulted in
233 morphological defects of *E. coli* cells (Fig. 4e and supplementary Fig. 5).
234
235 To study the role of MreD in the elongasome, FRET experiments were
236 designed to detect a possible interaction with PBP2. The Ef_A value of 4.3 ±
237 1.1% indicated a direct interaction between MreD and PBP2 (Fig. 4c, Table 1
238 and Supplementary Fig. 3). Subsequently, the interaction between MreC and
239 PBP2 was measured by FRET in the presence of MreD. The calculated Ef_A
240 between MreC and PBP2 was significantly reduced from 5.1 ± 1.2% to 3.3 ±
241 0.5% ($p=0.0078$) when MreD was co-expressed (Fig. 4c, Table 1 and
242 Supplementary Fig. 3). Since MreC reduced the Ef_A of RodA-PBP2 from 8.8 ±
243 1.1% to 4.9 ± 0.5%, it was possible that MreD altered the effect of MreC on
244 the RodA-PBP2 interaction. Therefore, the three-plasmid FRET experiment
245 was applied to detect the interaction between RodA and PBP2 in the
246 presence of MreCD. Interestingly, the Ef_A value of RodA-PBP2 was restored
247 to 9.2 ± 1.5%, which was comparable with the Ef_A in the presence of the third,
248 empty plasmid (Fig. 4d and Table 2). These combined results suggest a

regulatory mechanism by which MreC interacts with PBP2 and changes its conformation, while MreD interacts with MreC and PBP2 to prevent this conformational change PBP2. These conformational changes could correspond the proposed on and off states of PBP2 as published (44) (Fig. 4 a and b).

The cytoplasmic part of PBP2 is important for the interplay with the MreCD proteins

As showed before, the cytoplasmic NT part of PBP2 has an essential unknown function rather than being involved in the RodA-PBP2 interaction (Fig. 3). We considered that the NT of PBP2 might be important for its self-interaction and or interactions with other partner proteins. However, the Ef_A values of ^{MalFNT}PBP2 with wild type PBP2, MreC and MreD were not different from those of wild type PBP2 (Fig. 4d, Supplementary Fig. 7 and Table 1). Interestingly, the Ef_A value of the interaction between MreC and wild type PBP2, but not the ^{MalFNT}PBP2, was reduced by the co-expression of MreD (Fig. 4d, Table 1 and Supplementary Fig. 4c). Similarly, in the three-plasmid FRET experiments, MreD was not able to suppress the MreC-mediated change in the ^{MalFNT}PBP2-RodA interaction; the Ef_A value of RodA-^{MalFNT}PBP2 FRET remained at 5.5 ± 1.7% in presence of MreCD, rather than being restored to 9.2 ± 1.5% as in the RodA-PBP2^{WT} experiments (Fig. 4d, Table 2 and Supplementary Fig. 4c). Together, these results indicate that the cytoplasmic part of PBP2 plays an important role in the MreCD-mediated regulation of the interaction between PBP2 and RodA.

MreCD proteins do not alter PBP2 self-interaction

So far our results has shown that MreC and MreD have opposite effects on the interaction between RodA and PBP2. In contrast, the interaction between two PBP2 molecules (17) was not significantly affected upon overexpression of MreC or MreCD, as the calculated Ef_A values for the PBP2-PBP2 interaction remained unchanged compared to the values for the expression of the third empty plasmid (Fig. 4d and Table 2). RodA was also found to interact with itself (Table 1 and Supplementary Fig. 7). Likely PBP2 and RodA function as a complex of dimers, which might also allow simultaneously synthesis of multiple glycan strand as has been proposed (47–49).

Effect of mecillinam on the interaction between RodA and PBP2

As showed above, both the transmembrane helix and periplasmic part of PBP2 contribute to its interaction with RodA (Fig. 3). The binding of MreC to the periplasmic hydrophobic zipper domain of PBP2, which presumably changes the conformation of PBP2 from off state to on state, reduces the detected Ef_A between RodA and PBP2 (Fig. 4d and e). Interestingly, the PBP2 specific inhibitor mecillinam, also caused a reduction in the FRET efficiency of the interaction between RodA and PBP2. The RodA-$PBP2^{WT}$ interaction pair yielded a reduced Ef_A of 8.6 ± 1.1% in the presence of mecillinam (33), comparing with the Ef_A of 12.7 ± 1.7% without mecillinam (Fig. 2, Table 1 and Supplementary Fig. 8). Since mecillinam binds specifically to the periplasmic TPase active site of PBP2, a possible explanation could be that binding of mecillinam reduces the affinity between the periplasmic parts of PBP2 and RodA, but does not interfere with the interaction between their

transmembrane regions. Indeed, after replacing the transmembrane helix of PBP2 to abolish this part of the interaction (RodA-^{MalF37}PBP2), mecilinam further reduced the Ef_A value to 3.0 ± 2.0% (Supplementary Fig. 8 and Table 1), consistent with an almost complete loss of the interaction between RodA and ^{MalF37}PBP2. That mecillinam causes disruption of only one out of two interacting regions between PBP2 and RodA is also in agreement with the observations that it does not disrupt the structure of the elongasome (50). The inactive mutant PBP2^{S330C}, which cannot bind benzylpenicillin (35), still responded to mecillinam and showed a similar Ef_A reduction as PBP2^{WT} (Supplementary Fig. 8 and Table 1). This suggests that although the inactive mutant PBP2^{S330C} does not bind mecillinam covalently, it still interacts with it.

PBP2^{L61R} stays in the off state and activates RodA

A recent study reported a version of PBP2 in which Leu61 was replaced by Arg (PBP2^{L61R}) that could suppress an MreC defect, and was proposed to stay in the on state conformation mimicking activation by MreC (51). If this would be the case, the RodA-PBP2^{L61R} pair would be expected to have a reduced FRET efficiency, since the MreC activated RodA-PBP2^{WT} pair resulted in a reduction in FRET efficiency (Fig 4d). Therefore, we constructed an N-terminal mKO fusion of PBP2^{L61R} to test the interactions with its partner proteins. Surprisingly, the Ef_A for RodA-PBP2^{L61R} remained 12.8 ± 2.8%, which was comparable with the Ef_A of RodA-PBP2^{WT} that was presumably in the off state (Fig. 5a and b, Table 1 and Supplementary Fig. 9a). Mecillinam reduces the Ef_A value of the RodA-PBP2^{L61R} interaction to 9.7± 2.2%, which was also comparable with its effect on the RodA-PBP2^{WT} interaction (Table 1

and Fig. S8), indicating that the TPase active side of PBP2^{L61R} is still accessible to mecillinam. Unfortunately, the co-expression of PBP2^{L61R} together with either MreC or MreD alone, or both together, was not possible in most cases, as FRET cells repeatedly lost the mKO-PBP2^{L61R} signal upon induction (Table 1), suggesting toxicity of these combinations. The cells did not lose the mKO signal in only two out of six attempts to co-express MreC and PBP2^{L61R}. Of those samples the calculated Ef_A value of the MreC and PBP2^{L61R} pair remained at 5.4 ± 1.7%, which was comparable with MreC-PBP2^{WT} (Fig. 4a and Table 1). These results suggest that the hyperactive mutant PBP2^{L61R} likely behaves similarly as wild type PBP2 in the interaction with its partner proteins.

Having observed these unexpected results, we continued to further characterize the hyperactive PBP2^{L61R}. Consistent with its reported functionality (51), we observed that mKO-PBP2^{L61R} was capable to support growth of the PBP2(TS) strain LMC582 at the non-permissive temperature (Supplementary Fig. 9b). However, the expression of mKO-PBP2^{L61R} resulted in longer and thinner cells (Fig. 5c and Supplementary Fig. 9c), and in reduced sensitivity of cells to the MreB inhibitor A22 (Fig. 5c) as reported (51). Interestingly, cells expressing PBP2^{L61R} were hypersensitive to mecillinam (Fig. 5c and d). These results indicate potential defects in the peptidoglycan layer of cells expressing PBP2^{L61R}, and these defects may be tolerable under undisturbed growth conditions but are exacerbated in the presences of mecillinam. Considering that PBP2^{L61R} stimulates the GTase activity of RodA *in vitro* (51) and our results on the cellular interactions, it was possible that the

L61R exchange in PBP2 enhances only the activity of RodA and has no effect on PBP2's TPase activity. *In vitro* peptidoglycan synthesis experiments showed that inactivation of PBP2 by mecillinam resulted in longer glycan chains synthesized by a PBP1A-PBP2 complex (18), hence we wondered whether the presence of PBP2^{L61R} affected peptidoglycan synthesis in the cell. We prepared peptidoglycan and analyzed its composition from cells expressing PBP2^{L61R}, wild type PBP2, and the control membrane protein GlpT. As predicted, the peptidoglycan from all strains retained a similar extent of peptide cross-linkage. By contrast, only the peptidoglycan from the PBP2^{L61R} expressing cells contained unusually long glycan chains with a mean length ~52 disaccharide units (Table 3). The peptidoglycan of the strain overexpressing wild-type PBP2 had a mean glycan chain length of ~38 units, and the mean glycan chain lengths of the other strains were between 40-43 disaccharide units (Table 3, Supplementary Table 3). A stimulating effect of PBP2^{L61R} on RodA's GTase activity would be consistent with the previously observed A234T mutation in RodA that suppressed the morphological defects of MreC mutants (51), and would also explain why PBP2^{L61R} could only poorly restore survival and rod-shape in cells depleted of MreCD or RodZ (51). The tolerance to A22 and changes in MreB dynamics in the PBP2^{L61R} background (51) could also be explained by the enhanced RodA GTase activity by PBP2^{L61R}; a direct interaction between RodA and MreB was detected with a Ef_A value of 5.5% ± 1.7% (Table 1 and Supplementary Fig. 10). All together these results indicate that the 'hyperactive' PBP2^{L61R} likely has unchanged TPase activity itself but is probably in the off state conformation in the absence of MreC (44). The changes in cell morphology, the resistance to A22

and sensitivity to mecillinam, the partial compensation of MreCD-RodZ depletion and MreB dynamic changes are all likely due to an enhanced GTase activity of RodA (and perhaps PBP1A) (18, 51), which results into longer glycan chains in the peptidoglycan mesh.

Discussion

Peptidoglycan synthesis by the elongasome and divisome

In this work we aimed to reveal the regulation of peptidoglycan synthesis during length growth. Recent studies revealed a possible mechanism for the regulation of septal peptidoglycan synthesis by FtsBLQ and FtsN (19–21, 52–54). In this model, the FtsBLQ subcomplex inhibits the activities of PBP3 (consequently also inhibiting FtsW) and PBP1B, and keeps septal peptidoglycan synthesis in check. A small amount of FtsN is already present at pre-septal sites together with ZipA and the class A PBPs, PBP1A and PBP1B (55). However, only once FtsN accumulates at higher levels it is able to relieve the suppression of FtsBLQ on the peptidoglycan synthases, thereby activating septal peptidoglycan synthesis. During length growth, the elongasome proteins, such as MreC, MreD, PBP2, RodA and RodZ, localize in the lateral membrane, which makes it a challenge to investigate their cellular dynamics. Thus, it is still largely unknown how the elongasome regulates and coordinates peptidoglycan synthesis.

MreCD proteins regulate the interaction between RodA and PBP2

In this study, we showed that RodA and PBP2 form a subcomplex independent of their biochemical activities (Fig. 2). This interaction requires

399 the transmembrane helix and periplasmic parts of PBP2 (Fig. 3). *In vivo* FRET
400 experiments revealed that MreC interacts with directly with PBP2, which
401 modulated the interaction between PBP2 and RodA (Fig. 4). Surprisingly,
402 MreD also interacts with PBP2 and but has an opposite effect, as it reverses
403 the PBP2-RodA interaction change stimulated by MreC (Fig. 4). This is similar
404 to the regulation of septal peptidoglycan synthesis where FtsN interacts with
405 itself and accumulates at midcell (56, 57), and this accumulation is assumed
406 to abolish the suppression of the peptidoglycan synthesis complex FtsW-
407 PBP3-PBP1B by FtsBLQ. When comparing the cellular numbers of these
408 proteins synthesized per generation (46), we noticed that the average number
409 of FtsN molecules per cell is about 2 times higher than that of FtsBLQ and
410 FtsW-PBP3 proteins. The number of MreC molecules is also about 2 times
411 higher than that of MreD and PBP2-RodA molecules (46). MreC, but not MreD,
412 is also reported to interact with itself, and the structural data showed that two
413 molecules of MreC bind to one PBP2 molecule (44). Together with these
414 published data, our results indicate that the balance between the MreC and
415 MreD determines the nature of the interaction between PBP2 and RodA.
416 Structural data show that the interaction between MreC and PBP2 causes a
417 conformational change in PBP2 that was suggested to correspond to its
418 activation from the off state to the on state (44). This conformational change
419 could correspond to the change in the interaction between PBP2 and RodA
420 induced by MreC. And likely, when MreD is co-expressed with MreC, the
421 reversed change in the interaction between PBP2 and RodA could
422 correspond to the PBP2 conformational change from the on state to the off
423 state. This potential of MreC and MreD to affect the RodA-PBP2 interaction

424 could reflect the regulation of elongasome activity and peptidoglycan
425 synthesis during length growth. The overexpression of either MreC or MreD
426 would shift this balance and result in over activation or suppression of PBP2-
427 RodA activities, and cause morphological defects (Fig. 4e and Supplementary
428 Fig. 7).

429 Based on our observations, we propose a model for the regulation of
430 PBP2 (elongasome) activity and cylindrical peptidoglycan synthesis (Fig. 6).
431 The peptidoglycan synthases RodA and PBP2 form a stable subcomplex.
432 MreC stimulates and activates PBP2 and RodA, while MreD interferes with
433 the PBP2 MreC interaction to keep PBP2 activity and peptidoglycan synthesis
434 in check. The further binding and accumulation of MreC to PPB2 would
435 eventually outcompete MreD, which will activate PBP2 and consequently
436 initiate peptidoglycan synthesis. Because hydrolytic activity is required to
437 allow insertion of newly synthesized peptidoglycan into the existing mesh (58,
438 59), a balanced regulation is likely needed to avoid premature glycan strand
439 synthesis. Consequently, the elonsasome, like the divisome, must have a
440 mechanism to sense whether all partners are at the right position to act. A
441 well-regulated moment for the switching on of peptidoglycan synthesis by
442 balancing the MreCD ration is likely part of such a regulatory system.
443

444 **Materials and Methods**

445 **Media, strains, plasmids and primers**

446 LB (10 g tryptone, 5 g yeast extract and 10 g NaCl, per liter) and Gb4 (6.33g
447 $K_2HPO_4 \cdot 3H_2O$, 2.95g KH_2PO_4, 1.05 g $(NH_4)_2SO_4$, 0.10 g $MgSO_4 \cdot 7H_2O$, 0.28
448 mg $FeSO_4 \cdot 7H_2O$, 7.1 mg $Ca(NO_3)_2 \cdot 4H_2O$, 4 mg thiamine, 2 mg uracil, 2 mg

lysine, 2 mg thymine, and 0.5 % glucose, per liter, pH 7.0) were used for cell cultures in rich and minimal medium, respectively, as indicated. Final concentrations for antibiotics were: 100 $\mu g \cdot L^{-1}$ ampicillin, 50 $\mu g \cdot L^{-1}$ kanamycin and 25 $\mu g \cdot L^{-1}$ chloramphenicol.

E. coli strains and plasmids used in this study are listed in supplementary Table 1. Primers used in this study were listed in supplementary Table 2. The plasmids were constructed as following:

pXL29. Plasmid pXL28 and pWA004 were digested with *EcoR*I and *Hind*III restriction enzymes, the generated *(*$(GGS)_2$-GlpT expressing gene and pSAV057-mKO linear vector were ligated together to generate the mKO-$(GGS)_2$-GlpT expressing plasmid.

pXL36, pXL40, pXL44, pXL48, pXL56 and pXL63. Plasmids pXL36 and pXL40 that expressing mCherry-fused $RodA^{R109A}$ and $RodA^{Q207R}$ were generated from pSAV047-RodA by mutagenesis PCR using primer pairs priXL61-priXL61 and priXL69-priXL70, respectively. To construct non-fused version of RodA variants, wild type *rodA* gene was amplified using primer priXL59 and priXL60 from the MG1655 genomic DNA and ligated into empty pSAV057 vector, to generate plasmid pXL63. The two mutants plasmids were generated in the same way as descripted above from pXL63. mKO fused RodA plasmid pXL56 was constructed by cutting and pasting the *rodA* gene from pSAV047-RodA to the pSAV058 plasmid with *EcoRI* and *HindIII* restriction enzymes.

474

475 ***pXL148, pXL149, pXL158 and pXL159***. The PBP2 domain swap plasmids
476 were constructed by Gibson assembly (60). For N-terminus replacement,
477 primer pairs priXL146-priXL258 and priXL147-priXL259 were used for PCR
478 from plasmid pWA004. The PCR products were purified after *DpnI* digestion
479 and assembled to generated pXL148 that excludes the N-terminus of PBP2.
480 For pXL149, the primer pair priXL258-priXL260 was used to amplify the entire
481 pWA004 plasmid excluding the first 45 residues. Primer pair priXL261 and
482 priXL263 was use to amplify the first 37 residues of MalF from MG1655
483 genome. The PCR products were purified after *DpnI* digestion and assembled
484 to generate pXL149 plasmid. The $PBP2^{S330C}$ and $PBP2^{L61R}$ plasmids were
485 constructed with mutagenesis PCR from the pWA004 plasmid using primer
486 pairs priXL274-priXL275 and priXL276-priXL277, respectively.

487

488 ***pXL165***, ***pXL166 and pXL169***. *mreC*, *mreCD* and *mreD* genes were
489 amplified from MG1655 genome using primer pairs priXL282-priXL286,
490 priXL282-priXL283 and priXL299-priXL283, respectively, and cloned into
491 plasmid pSAV047 with *EcoRI* and *HindIII* restriction enzymes, to generate the
492 mCherry fused version of these genes.

493

494

495 ***pXL167 and pXL168***. The third plasmids used in the three-plasmids FRET
496 experiments. *mreC* and *mreCD* genes were cloned into plasmid pSG4K5 (61)
497 with Gibson assembly, respectively, and the $p_{trcdown}$ promoter was introduced
498 to control the protein expression. Primer pair priXL294-priXL295 was used to

amplify the linear vector from pSG4K5. Primer pair priXL296-pp15 was used to amplify the $p_{trcdown}$ promoter. Primer pairs pXL284-priXL297 and priXL284-priXL298 were used to amplify the *mreCD* and *mreD* genes, respectively.

Bacterial growth, morphology and protein localization

For general growth experiments in rich medium, overnight cultures (37 °C) were diluted 1:1000 into fresh LB medium with 0.5% glucose and the required antibiotics, and grew to OD_{600} around 0.2 at 37 °C. Cultures were further diluted 1:5 into fresh LB medium with required antibiotics, and induced with 15 μM IPTG for 2 mass doubling at 37 °C (OD_{600} reached around 0.2).

For complementation experiments, temperature sensitive strains expressing the mutant plasmids were grown as described above at 30 °C. Cultures were further diluted 1:5 into fresh LB medium with required antibiotics, and induced with 15 μM IPTG for 2 mass doubling at 30 °C and 42 °C, respectively (OD_{600} reached around 0.2).

After induction, cells were fixed with FAGA (2.8 % formaldehyde and 0.04 % glutaraldehyde, final concentration) for 15 minutes and centrifuged at 7000 rpm for 10 min at room temperature. Cell pellets were suspended and washed 3 times with PBS (pH7.2) buffer. Subsequently, bacterial morphology and protein localization were imaged by wide field phase contrast and fluorescence microscopy. Specially, cells expressing the mKO fused proteins were firstly matured at 37 °C overnight before imaging by microscopy.

FRET experiment and data analysis

Protein interactions were detected by FRET as described previously (33, 37, 62). For the FRET experiments, mCherry and mKO fluorescent proteins were used as acceptor and donor fluorophores, respectively. LMC500 strain was co-transformed with the FRET pairs that were to be detected. In each FRET experiment, the empty-vector reference, mCherry reference, mKO reference were included to be able to calculate the Ef_A by unmixing of the measured FRET pair spectrum in its individual components; background, mCherry, mKO and sensitized emission spectra. A tandem fusion of mKO-mCherry was used as positive control, and the mCherry-RodA and mKO-GlpT pair was used as negative control. After transformation, FRET strains were firstly grown in LB medium (with antibiotics and 0.5% glucose) overnight at 37 °C, and diluted 1:1000 into fresh medium and grown to OD_{600} around 0.2 at 37 °C. Subsequently, FRET strains were diluted 1:500 into Gb4 medium and grown to steady state at 28 °C (OD_{450} was kept below 0.2). All FRET strains were induced with 15 μM IPTG (and treated with mecillinam at 2 $mg \cdot L^{-1}$ concentration as indicated) for two mass doubling before FAGA fixation. After fixation, FRET cells were pelleted by centrifugation at 7000rpm at room temperature and washed 3 times with PBS buffer (pH 7.2). Then all samples were incubated at 37 °C overnight and stored at 4 °C for 1 extra day before measured with spectrofluorimeter (Photon Technology International, NJ). Emission spectra of acceptor and donor fluorophores were measured through 6-nm slit widths with 1 second integration time per scanned nm for 3 times averaging. Filters 587/11 nm (587/11 nm BrightLine single band-pass filter, Semrock, New York, NY, USA) and 600nm long-pass (LP) filter (Chroma

549 Technology Corp., Bellows Falls, VT) were used for excitation and emission of
550 acceptor fluorophore (mCherry), while 541/12 nm (Semrock) and 550 nm long
551 pass (Chroma) filters were used for mKO excitation and emission,
552 respectively. For calculation, measurement of PBS buffer was subtracted from
553 all samples, and the empty-cell reference was subtracted from the donor and
554 acceptor spectra. The FRET efficiencies were calculated as described
555 previously (37, 62).
556
557 For three plasmids FRET, a third plasmid (expressing MreC or expressing
558 MreCD both) was introduced into the whole two plasmids FRET system.
559 Empty pSG4K5 vector was also introduced as a control to correct for the
560 reduction in FRET efficiency due to the burden of maintaining three plasmids.
561
562 **Spot assay**
563 To test the sensitivity of *E. coli* strains to A22 and mecillinam, LMC500 strain
564 was transformed with pWA004 ($PBP2^{WT}$) or pXL159 ($PBP2^{L61R}$). Strains
565 expressing each construct were grown in LB medium as descried above
566 without induction. Cell cultures were diluted with varying dilution factors (Fig.
567 4C). A drop of 10 µl cell culture from each dilution was loaded on the LB agar
568 dish (with chloramphenicol, 15 µM IPTG, 10 $\mu g \cdot mL^{-1}$ A22 or 2 $\mu g \cdot mL^{-1}$
569 mecillinam) and incubated overnight at 37 °C.
570
571 **Peptidoglycan analysis**
572 Peptidoglycan sacculi were prepared from *E. coli* cells, digested with cellosyl
573 (kind gift from Hoechst, Germany), reduced with sodium borohydride and

574 analyzed by high pressure liquid chromatography as described (Separation
575 and quantification of muropeptides with high-performance liquid
576 chromatography) (63).
577
578 **Microscopy**
579 Bacterial cell samples were immobilized on 1.3% agarose pads (w/v in Gb4
580 medium) and imaged under microscopy. Fluorescence microscopy was
581 carried out either with an Olympus BX-60 fluorescence microscope equipped
582 with an UPlanApo 100×/N.A. 1.35 oil Iris Ph3 objective, or with a Nikon
583 Eclipse Ti microscope equipped with a C11440-22CU Hamamatsu ORCA
584 camera, a CFI Plan Apochromat DM 100× oil objective, an Intensilight HG
585 130W lamp and the NIS elements software (version 4.20.01). Images were
586 acquired using the Micro Manager 1.4 plugin for ImageJ, and analyzed with
587 Coli-Inspector supported by the ObjectJ plugin for ImageJ (version 1.49v) (64).
588
589
590 **Acknowledgements**
591 X.L. was supported by the Chinese Scholarship Council (File
592 No.201406220123). W.V. received funding from the Wellcome Trust
593 (101824/Z/13/Z). We thank Lisa Atkinson for preparation of peptidoglycan
594 sacculi and Prof. Thomas Bernhardt for the gift of modeled *E. coli* PBP2
595 structures(51).
596
597
598

Author contributions

X.L and T.B. designed and analyzed all the experiments. X.L. performed all experiments. Jacob Biboy and Waldemar Vollmer performed the peptidoglycan analysis experiment and analyzed these data. X.L. and T.B. analyzed all FRET data and wrote the manuscript.

Conflicting interests

The authors declare no conflicting interests.

References

1. Vollmer W, Blanot D, De Pedro MA. 2008. Peptidoglycan structure and architecture. FEMS Microbiol Rev 32:149–167. https://doi.org/10.1111/j.1574-6976.2007.00094.x
2. Mengin-Lecreulx D, Flouret B, Van Heijenoort J. 1982. Cytoplasmic steps of peptidoglycan synthesis in *Escherichia coli*. J Bacteriol 151:1109–1117. https://doi.org/10.1111/j.1574-6976.2008.00104.x
3. Bouhss A, Trunkfield AE, Bugg TDH, Mengin-Lecreulx D. 2008. The biosynthesis of peptidoglycan lipid-linked intermediates. FEMS Microbiol Rev. https://doi.org/10.1111/j.1574-6976.2007.00089.x
4. van Heijenoort J. 2007. Lipid Intermediates in the Biosynthesis of Bacterial Peptidoglycan. Microbiol Mol Biol Rev 71:620–635. https://doi.org/10.1128/MMBR.00016-07
5. Mohammadi T, Sijbrandi R, Lutters M, Verheul J, Martin NI, Den Blaauwen T, De Kruijff B, Breukink E. 2014. Specificity of the transport of lipid II by FtsW in *Escherichia coli*. J Biol Chem 289:14707–14718. doi:10.1074/jbc.M114.557371
6. Sham L-T, Butler EK, Lebar MD, Kahne D, Bernhardt TG, Ruiz N. 2014. MurJ is the flippase of lipid-linked precursors for peptidoglycan biogenesis. Science (80-) 345:220–222. https://doi.org/10.1126/science.1254522
7. Sieger B, Schubert K, Donovan C, Bramkamp M. 2013. The lipid II flippase RodA determines morphology and growth in *Corynebacterium glutamicum*. Mol Microbiol 90:966–982. https://doi.org/10.1111/mmi.12411
8. Sauvage E, Kerff F, Terrak M, Ayala JA, Charlier P. 2008. The penicillin-binding proteins: Structure and role in peptidoglycan biosynthesis. FEMS Microbiol Rev 32:234–258. https://doi.org/10.1111/j.1574-6976.2008.00105.x

9. Meeske AJ, Riley EP, Robins WP, Uehara T, Mekalanos JJ, Kahne D, Walker S, Kruse AC, Bernhardt TG, Rudner DZ. 2016. SEDS proteins are a widespread family of bacterial cell wall polymerases. Nature 1–15. https://doi.org/10.1038/nature19331
10. Taguchi A, Welsh MA, Marmont LS, Lee W, Sjodt M, Kruse AC, Kahne D, Bernhardt TG, Walker S. 2019. FtsW is a peptidoglycan polymerase that is functional only in complex with its cognate penicillin-binding protein. Nat Microbiol. https://doi.org/10.1038/s41564-018-0345-x
11. Den Blaauwen T, De Pedro MA, Nguyen-Distèche M, Ayala JA. 2008. Morphogenesis of rod-shaped sacculi. FEMS Microbiol Rev 32:321–344. https://doi.org/10.1111/j.1574-6976.2007.00090.x
12. Pichoff S, Lutkenhaus J. 2005. Tethering the Z ring to the membrane through a conserved membrane targeting sequence in FtsA. Mol Microbiol 55:1722–1734. https://doi.org/10.1111/j.1365-2958.2005.04522.x
13. Schmidt KL, Peterson ND, Kustusch RJ, Wissel MC, Graham B, Phillips GJ, Weiss DS. 2004. A Predicted ABC Transporter , FtsEX , Is Needed for Cell Division in *Escherichia coli*. J Bacteriol 186:785–793. https://doi.org/10.1128/JB.186.3.785-793.2004
14. Hale CA, De Boer PAJ. 1997. Direct binding of FtsZ to ZipA, an essential component of the septal ring structure that mediates cell division in *E. coli*. Cell 88:175–185. https://doi.org/10.1016/S0092-8674(00)81838-3
15. Aarsman MEG, Piette A, Fraipont C, Vinkenvleugel TMF, Nguyen-Distèche M, Den Blaauwen T. 2005. Maturation of the *Escherichia coli* divisome occurs in two steps. Mol Microbiol 55:1631–1645. https://doi.org/10.1111/j.1365-2958.2005.04502.x
16. den Blaauwen T, Hamoen LW, Levin PA. 2017. The divisome at 25: the road ahead. Curr Opin Microbiol 36:85–94. https://doi.org/10.1016/j.mib.2017.01.007
17. Van der Ploeg R, Verheul J, Vischer NOE, Alexeeva S, Hoogendoorn E, Postma M, Banzhaf M, Vollmer W, Den Blaauwen T. 2013. Colocalization and interaction between elongasome and divisome during a preparative cell division phase in *Escherichia coli*. Mol Microbiol 87:1074–1087. https://doi.org/10.1111/mmi.12150
18. Banzhaf M, van den Berg van Saparoea B, Terrak M, Fraipont C, Egan A, Philippe J, Zapun A, Breukink E, Nguyen-Distèche M, den Blaauwen T, Vollmer W. 2012. Cooperativity of peptidoglycan synthases active in bacterial cell elongation. Mol Microbiol 85:179–194. https://doi.org/10.1111/j.1365-2958.2012.08103.x
19. Ranjit DK, Jorgenson MA, Young KD. 2017. PBP1B Glycosyltransferase and Transpeptidase Activities Play Different Essential Roles during the De Novo Regeneration of Rod Morphology in *Escherichia coli*. J Bacteriol 199:1–17. https://doi.org/10.1128/JB.00612-16
20. den Blaauwen T, Luirink J. 2019. Checks and Balances in Bacterial Cell Division. MBio 10:1–6. https://doi.org/10.1128/mBio.00149-19
21. Boes A, Olatunji S, Breukink E, Terrak M. 2019. Regulation of the peptidoglycan polymerase activity of PBP1b by antagonist actions of the core divisome proteins FtsBLQ and FtsN. MBio 10:1–16.

https://doi.org/10.1128/mBio.01912-18
22. Egan AJF, Biboy J, van't Veer I, Breukink E, Vollmer W. 2015. Activities and regulation of peptidoglycan synthases. Philos Trans R Soc B Biol Sci 370:20150031. https://doi.org/10.1098/rstb.2015.0031
23. van Teeffelen S, Wang S, Furchtgott L, Huang KC, Wingreen NS, Shaevitz JW, Gitai Z. 2011. The bacterial actin MreB rotates, and rotation depends on cell-wall assembly. Proc Natl Acad Sci 108:15822–15827. https://doi.org/10.1073/pnas.1108999108
24. Errington J. 2015. Bacterial morphogenesis and the enigmatic MreB helix. Nat Rev Micro 13:241–248. https://doi.org/10.1038/nrmicro3398
25. White CL, Gober JW. 2012. MreB: Pilot or passenger of cell wall synthesis? Trends Microbiol 20:74–79. https://doi.org/10.1016/j.tim.2011.11.004
26. Strahl H, Bürmann F, Hamoen LW. 2014. The actin homologue MreB organizes the bacterial cell membrane. Nat Commun 5:1–11. https://doi.org/10.1038/ncomms4442
27. Garner EC, Bernard R, Wang W, Zhuang X, Rudner DZ, Mitchison T. 2011. Coupled, circumferential motions of the cell wall synthesis machinery and MreB filaments in *B. subtilis*. Science (80-) 333:222–5. https://doi.org/10.1126/science.1203285
28. Bendezú FO, Hale CA, Bernhardt TG, De Boer PAJ. 2009. RodZ (YfgA) is required for proper assembly of the MreB actin cytoskeleton and cell shape in *E. coli*. EMBO J 28:193–204. https://doi.org/10.1038/emboj.2008.264
29. Ikebe R, Kuwabara Y, Chikada T, Niki H, Shiomi D. 2018. The periplasmic disordered domain of RodZ promotes its self-interaction in *Escherichia coli*. Genes to Cells 23:307–317. https://doi.org/10.1111/gtc.12572
30. Kruse T, Bork-Jensen J, Gerdes K. 2005. The morphogenetic MreBCD proteins of *Escherichia coli* form an essential membrane-bound complex. Mol Microbiol 55:78–89. https://doi.org/10.1111/j.1365-2958.2004.04367.x
31. Colavin A, Shi H, Huang KC. 2018. RodZ modulates geometric localization of the bacterial actin MreB to regulate cell shape. Nat Commun 9:1280. https://doi.org/10.1038/s41467-018-03633-x
32. Morgenstein RM, Bratton BP, Nguyen JP, Ouzounov N, Shaevitz JW, Gitai Z. 2015. RodZ links MreB to cell wall synthesis to mediate MreB rotation and robust morphogenesis. Proc Natl Acad Sci U S A 112:12510–12515. https://doi.org/10.1073/pnas.1509610112
33. van der Ploeg R, Goudelis ST, den Blaauwen T. 2015. Validation of FRET assay for the screening of growth inhibitors of *Escherichia coli* reveals elongasome assembly dynamics. Int J Mol Sci 16:17637–17654. https://doi.org/10.3390/ijms160817637
34. Emami K, Guyet A, Kawai Y, Devi J, Wu LJ, Allenby N, Daniel RA, Errington J. 2017. RodA as the missing glycosyltransferase in *Bacillus subtilis* and antibiotic discovery for the peptidoglycan polymerase pathway. Nat Microbiol 2:1–8. https://doi.org/10.1038/nmicrobiol.2016.253
35. Takasuga A, Adachi H, Ishino F, Matsuhashi M, Ohta T, Matsuzawa H. 1988. Identification of the penicillin-binding active site of penicillin-

738 binding protein 2 of *Escherichia coli*. J Biochem 104:822–826.
739 https://doi.org/10.1093/oxfordjournals.jbchem.a122556
740 36. Cho H, Wivagg CN, Kapoor M, Barry Z, Rohs PDA, Suh H, Marto JA,
741 Garner EC, Bernhardt TG. 2016. Bacterial cell wall biogenesis is
742 mediated by SEDS and PBP polymerase families functioning semi-
743 Autonomously. Nat Microbiol 1.
744 https://doi.org/10.1038/nmicrobiol.2016.172
745 37. Meiresonne NY, van der Ploeg R, Hink MA, den Blaauwen T. 2017.
746 Activity-related conformational changes in D,D-carboxypeptidases
747 revealed by in vivo periplasmic förster resonance energy transfer assay
748 in *Escherichia coli*. MBio 8:1–18. https://doi.org/10.1128/mBio.01089-17
749 38. Pastoret S, Fraipont C, Blaauwen T Den, Aarsman MEG, Thomas A,
750 Brasseur R, Nguyen-diste M. 2004. Functional analysis of the cell
751 division protein FtsW of *Escherichia coli*. J Bacteriol 186:8370–8379.
752 https://doi.org/10.1128/JB.186.24.8370-8379.2004
753 39. Oldham ML, Khare D, Quiocho FA, Davidson AL, Chen J. 2007. Crystal
754 structure of a catalytic intermediate of the maltose transporter. Nature
755 450:515–521. https://doi.org/10.1038/nature06264
756 40. Goehring NW, Robichon C, Beckwith J. 2007. Role for the nonessential
757 N terminus of FtsN in divisome assembly. J Bacteriol 189:646–649.
758 https://doi.org/10.1128/JB.00992-06
759 41. Meiresonne NY, Consoli E, Mertens LMY, Chertkova AO, Goedhart J,
760 den Blaauwen T. 2019. Superfolder mTurquoise2 ox optimized for the
761 bacterial periplasm allows high efficiency *in vivo* FRET of cell division
762 antibiotic targets. Mol Microbiol 111:1025–1038.
763 https://doi.org/10.1111/mmi.14206
764 42. Müller SM, Galliardt H, Schneider J, Barisas BG, Seidel T. 2013.
765 Quantification of Förster resonance energy transfer by monitoring
766 sensitized emission in living plant cells. Front Plant Sci 4:1–20.
767 https://doi.org/10.3389/fpls.2013.00413
768 43. Pauling L, Corey RB, Branson HR. 1951. The Structure of Proteins:
769 Two Hydrogen-Bonded Helical Configurations of the Polypeptide Chain.
770 Proc Natl Acad Sci U S A 37:205–211. doi: 10.1073/pnas.37.4.205
771 44. Contreras-Martel C, Martins A, Ecobichon C, Trindade DM, Matteï P-J,
772 Hicham S, Hardouin P, Ghachi M El, Boneca IG, Dessen A. 2017.
773 Molecular architecture of the PBP2–MreC core bacterial cell wall
774 synthesis complex. Nat Commun 8:776. https://doi.org/10.1038/s41467-
775 017-00783-2
776 45. Alexeeva S, Gadella TWJ, Verheul J, Verhoeven GS, Den Blaauwen T.
777 2010. Direct interactions of early and late assembling division proteins
778 in *Escherichia coli* cells resolved by FRET. Mol Microbiol 77:384–398.
779 https://doi.org/10.1111/j.1365-2958.2010.07211.x
780 46. Li GW, Burkhardt D, Gross C, Weissman JS. 2014. Quantifying
781 absolute protein synthesis rates reveals principles underlying allocation
782 of cellular resources. Cell 157:624–635.
783 https://doi.org/10.1016/j.cell.2014.02.033
784 47. Scheffers D-J, Pinho MG. 2005. Bacterial Cell Wall Synthesis: New
785 Insights from Localization Studies. Microbiol Mol Biol Rev 69:585 LP –
786 607. https://doi.org/10.1128/MMBR.69.4.585-607.2005
787 48. Holtje J V. 1998. Growth of the stress-bearing and shape-maintaining

murein sacculus of *Escherichia coli*. Microbiol Mol Biol Rev 62:181–203.
49. Holtje J-V. 1996. A hypothetical holoenzyme involved in the replication of the murein sacculus of *Escherichia coli*. Microbiology 142:1911–1918. https://doi.org/10.1099/13500872-142-8-1911
50. Karczmarek A, Baselga RMA, Alexeeva S, Hansen FG, Vicente M, Nanninga N, Den Blaauwen T. 2007. DNA and origin region segregation are not affected by the transition from rod to sphere after inhibition of *Escherichia coli* MreB by A22. Mol Microbiol 65:51–63. https://doi.org/10.1111/j.1365-2958.2007.05777.x
51. Rohs PDA, Buss J, Sim SI, Squyres GR, Srisuknimit V, Smith M, Cho H, Sjodt M, Kruse AC, Garner EC, Walker S, Kahne DE, Bernhardt TG. 2018. A central role for PBP2 in the activation of peptidoglycan polymerization by the bacterial cell elongation machinery. PLoS Genet 14:1–25. https://doi.org/10.1371/journal.pgen.1007726
52. Kureisaite-Ciziene D, Varadajan A, McLaughlin SH, Glas M, Montón Silva A, Luirink R, Mueller C, den Blaauwen T, Grossmann TN, Luirink J, Löwe J. 2018. Structural Analysis of the Interaction between the Bacterial Cell Division Proteins FtsQ and FtsB. MBio 9. https://doi.org/10.1128/mBio.01346-18
53. Egan AJF, Jean NL, Koumoutsi A, Bougault CM, Biboy J, Sassine J, Solovyova AS, Breukink E, Typas A, Vollmer W, Simorre J-PJ-P. 2014. Outer-membrane lipoprotein LpoB spans the periplasm to stimulate the peptidoglycan synthase PBP1B. Proc Natl Acad Sci U S A 111:8197–202. https://doi.org/10.1073/pnas.1400376111
54. Müller P, Ewers C, Bertsche U, Anstett M, Kallis T, Breukink E, Fraipont C, Terrak M, Nguyen-Distèche M, Vollmer W. 2007. The essential cell division protein FtsN interacts with the murein (peptidoglycan) synthase PBP1B in *Escherichia coli*. J Biol Chem 282:36394–36402. doi: 10.1074/jbc.M706390200
55. Pazos M, Peters K, Casanova M, Palacios P, VanNieuwenhze M, Breukink E, Vicente M, Vollmer W. 2018. Z-ring membrane anchors associate with cell wall synthases to initiate bacterial cell division. Nat Commun 9:5090. https://doi.org/10.1038/s41467-018-07559-2
56. Lutkenhaus J. 2009. FtsN - Trigger for septation. J Bacteriol 191:7381–7382. https://doi.org/10.1128/JB.01100-09
57. Gerding MA, Liu B, Bendezú FO, Hale CA, Bernhardt TG, De Boer PAJ. 2009. Self-enhanced accumulation of FtsN at division sites and roles for other proteins with a SPOR domain (DamX, DedD, and RlpA) in *Escherichia coli* cell constriction. J Bacteriol 191:7383–7401. https://doi.org/10.1128/JB.00811-09
58. Singh SK, Parveen S, SaiSree L, Reddy M. 2015. Regulated proteolysis of a cross-link–specific peptidoglycan hydrolase contributes to bacterial morphogenesis. Proc Natl Acad Sci 112:10956–10961. https://doi.org/10.1073/pnas.1507760112
59. Singh SK, Saisree L, Amrutha RN, Reddy M. 2012. Three redundant murein endopeptidases catalyse an essential cleavage step in peptidoglycan synthesis of *Escherichia coli* K12. Mol Microbiol 86:1036–1051. https://doi.org/10.1111/mmi.12058
60. Gibson DG, Young L, Chuang R-Y, Venter JC, Hutchison CA, Smith HO. 2009. Enzymatic assembly of DNA molecules up to several hundred

kilobases. Nat Methods 6:343–345. https://doi.org/10.1038/nmeth.1318

61. Standage-Beier K, Zhang Q, Wang X. 2015. Targeted Large-Scale Deletion of Bacterial Genomes Using CRISPR-Nickases. ACS Synth Biol 4:1217–1225. https://doi.org/10.1021/acssynbio.5b00132

62. Meiresonne NY, Alexeeva S, van der Ploeg R, den Blaauwen T. 2018. Detection of Protein Interactions in the Cytoplasm and Periplasm of *Escherichia coli* by Förster Resonance Energy Transfer. Bio-protocol 8:e2697. DOI: 10.21769/BioProtoc.2697

63. Glauner B. 1988. Separation and quantification of muropeptides with high-performance liquid chromatography. Anal Biochem 172:451–464. https://doi.org/10.1016/0003-2697(88)90468-X

64. Vischer NOE, Verheul J, Postma M, van den Berg van Saparoea B, Galli E, Natale P, Gerdes K, Luirink J, Vollmer W, Vicente M, den Blaauwen T. 2015. Cell age dependent concentration of *Escherichia coli* divisome proteins analyzed with ImageJ and ObjectJ. Front Microbiol 6:1–18. https://doi.org/10.3389/fmicb.2015.00586

Table 1. Summary of the calculated acceptor FRET efficiencies (Ef_A) from spectral FRET measurements for listed samples.

	Proteins expressed				
Parameter	**pTHV037**	**pSAV057**	**Ef_A (%)**	**SD (%)**	**N[1]**
Positive control[2]					
Tandem	Empty plasmid	mKO-mCh	31.0	4.0	22
Negative control[3]					
RodA-GlpT	mCh-RodA	mKO-$(GGS)_2$-GlpT	1.1	3.5	24
Biological interactions					
RodA[4]-PBP2^{WT}	mCh-RodA	mKO-PBP2^{WT}	12.7	1.7	16
RodA^{R109A}-PBP2	mCh-RodA^{R109A}	mKO-PBP2^{WT}	12.5	1.9	4
RodA^{Q207R}-PBP2	mCh-RodA^{Q207R}	mKO-PBP2^{WT}	12.7	1.2	4
RodA-PBP2^{S330C}	mCh-RodA	mKO-PBP2^{S330C}	10.9	0.5	3
RodA-^{MalFNT}PBP2	mCh-RodA	mKO-^{MalFNT}PBP2	14.4	1.7	4
RodA-^{MalF37}PBP2	mCh-RodA	mKO-^{MalF37}PBP2	8.2	1.3	3
RodA-PBP2^{L61R}	mCh-RodA	mKO-PBP2^{L61R}	12.8	2.8	8
RodA-RodA^{WT}	mCh-RodA	mKO-RodA	5.5	1.4	4
MreB^{SW}-RodA	mCh-MreB^{SW5}	mKO-RodA	7.2	3.4	4
PBP2^{WT} -PBP2^{WT}	mCh-PBP2^{WT}	mKO-PBP2	9.2	0.5	4
PBP2-^{MalFNT}PBP2	mCh-PBP2^{WT}	mKO-^{MalFNT}PBP2	10.5	2.0	4
MreC-PBP2^{WT}	mCh-MreC	mKO-PBP2^{WT}	5.1	1.2	6
MreC-^{MalFNT}PBP2	mCh-MreC	mKO-^{MalFNT}PBP2	5.4	1.7	6
MreC-PBP2^{L61R}	mCh-MreC	mKO-PBP2^{L61R}	5.3	0.6	2
MreD-PBP2^{WT}	mCh-MreD	mKO-PBP2^{WT}	4.3	1.2	10
MreD-^{MalFNT}PBP2	mCh-MreD	mKO-^{MalFNT}PBP2	5.3	1.6	10
MreCD[6]-PBP2^{WT}	mCh-MreCD	mKO-PBP2^{WT}	3.3	0.5	6
MreCD[7]-^{MalFNT}PBP2	mCh-MreCD	mKO-^{MalFNT}PBP2	5.4	1.1	5
+ mecillinam					
Positive control					
Tandem	Empty vector	mKO-mCh	31.0	0.6	2
Negative control					
RodA-GlpT	mCh-RodA	mKO-$(GGS)_2$-GlpT	3.1	0.1	2
Biological interactions					
RodA-PBP2^{WT}	mCh-RodA	mKO-PBP2^{WT}	8.6	1.1	6
RodA-^{MalF37}PBP2	mCh-RodA	mKO-^{MalF37}PBP2	3.0	2.0	4
RodA-PBP2^{S330C}	mCh-RodA	mKO-PBP2^{S330C}	7.9	1.0	2
RodA-PBP2^{L61R}	mCh-RodA	mKO-PBP2^{L61R}	9.7	2.2	3

[1] No, number of biological repeats;
[2,3] Here all measured positive and negative controls are averaged. In the figures the controls are included that belong to the corresponding measurements.
[4] RodA without superscript represent the wild type version.
[5] mCh-MreB^{SW} is a sandwich fusion of MreB-mCherry-MreB (33).
[6,7] MreC and MreD were expressed from one plasmid, and MreC was fused to mCherry while MreD was non-fused.

Table 2. Summary of the calculated acceptor FRET (Ef_A) efficiencies from spectral FRET measurements for listed samples.

	FRET pairs		Third plasmid: Empty vector			Third plasmid: MreC			Third plasmid: MreCD		
Parameter	**pTHV037**	**pSAV057**	**Ef_A (%)**	**SD (%)**	**N**	**Ef_A (%)**	**SD (%)**	**N**	**Ef_A (%)**	**SD (%)**	**N**
Positive control											
Tandem	Empty vector	mKO-mCh	30.4	1.9	4	31.3	3.2	3	31.7	4.3	2
Negative control											
RodA-GlpT	mCh-RodA	mKO-$(GGS)_2$-GlpT	2.4	1.3	7	2.2	1.1	2	1.4	2.1	4
Biological interactions											
RodA-$PBP2^{WT}$	mCh-RodA	mKO-$PBP2^{WT}$	8.8	1.1	6	4.9	0.6	2	9.2	1.5	4
RodA-^{MalFNT}PBP2	mCh-RodA	mKO-^{MalFNT}PBP2	7.6	1.8	5	4.2	0,3	2	5.5	1.7	4
$PBP2^{WT}$-$PBP2^{WT}$	mCh-$PBP2^{WT}$	mKO-$PBP2^{WT}$	10.6	2.1	6	8.6	1.4	2	9.8	1,2	4
$PBP2^{WT}$-^{MalFNT}PBP2	mCh-$PBP2^{WT}$	mKO-^{MalFNT}PBP2	9.4	3.5	5	9.8	1.9	2	8.7	1.8	4

N, number of samples measured.

Table 3. Summary of muropeptide composition of LMC500 strains carrying no plasmid or different expression plasmids.

Muropeptides[2] or feature	Percent peak area (%)[1]				
	LMC500	LMC500 mKO	LMC500 mKO-PBP2^{WT}	LMC500 mKO-PBP2^{L61R}	LMC500 mKO-GlpT
Monomers (total)	52.6 ± 0.1	52.0 ± 0.0	52.1 ± 1.1	52.2 ± 0.9	52.2 ± 0.0
dipeptides	1.4 ± 0.0	1.6 ± 0.1	1.3 ± 0.1	1.2 ± 0.0	1.4 ± 0.0
tripeptides	5.0 ± 0.2	5.0 ± 0.0	5.0 ± 0.5	4.0 ± 0.3	4.7 ± 0.1
tetrapeptides	41.6 ± 0.0	41.0 ± 0.0	41.3 ± 0.5	43.3 ± 2.0	41.8 ± 0.2
anhydro	0.9 ± 0.0	1.0 ± 0.0	1.0 ± 0.0	0.7 ± 0.0	1.0 ± 0.0
LysArg	3.7 ± 0.4	3.4 ± 0.2	3.5 ± 0.5	3.0 ± 1.2	3.4 ± 0.5
Dimers (total)	40.5 ± 0.0	40.8 ± 0.0	40.2 ± 0.7	41.7 ± 0.9	40.7 ± 0.1
tetratripeptide	3.1 ± 0.3	3.0 ± 0.2	3.0 ± 0.1	2.2 ± 0.0	2.9 ± 0.1
tetratetrapeptide	36.0 ± 1.0	36.3 ± 0.2	35.0 ± 2.6	37.1 ± 2.7	36.0 ± 0.9
anhydro	2.0 ± 0.0	2.1 ± 0.0	2.2 ± 0.0	1.7 ± 0.0	2.0 ± 0.0
LysArg	1.6 ± 0.0	1.7 ± 0.1	1.5 ± 0.2	1.2 ± 0.2	1.6 ± 0.1
Trimers (Total)	4.4 ± 0.1	4.6 ± 0.1	4.8 ± 0.0	3.8 ± 0.0	4.5 ± 0.1
Dipeptides (total)	1.4 ± 0.0	1.6 ± 0.1	1.3 ± 0.1	1.2 ± 0.0	1.4 ± 0.0
Tripeptides (total)	7.2 ± 0.9	7.2 ± 0.2	7.6 ± 1.1	6.3 ± 0.7	7.0 ± 0.3
Tetrapeptides (total)	85.8 ± 0.1	85.8 ± 0.0	85.3 ± 0.1	87.7 ± 0.0	86.2 ± 0.0
Chain ends (anhydro)	2.3 ± 0.0	2.4 ± 0.0	2.5 ± 0.0	1.9 ± 0.0	2.3 ± 0.0
Glycan chain length (DS)[3]	42.8 ± 0.2	40.5 ± 0.0	38.3 ± 0.1	**52.1 ± 0.5**	41.6 ± 0.0
Degree of cross-linkage	23.2 ± 0.1	23.4 ± 0.0	23.3 ± 0.1	23.3 ± 0.2	23.3 ± 0.0
% Peptides in cross-links	47.4 ± 0.1	48.0 ± 0.0	48.0 ± 1.1	47.8 ± 0.9	47.8 ± 0.0

[1] values are mean ± variation of two biological replicates.

[2] muropeptide names according to Glauner, 1988 (63).

[3] average glycan chain length in disaccharide (DS) units calculated from the percentage of anhydro-Mur*N*Ac containing muropeptides. The bold number highlights the increased average glycan chain length in cells expressing PBP2^{L61R}.

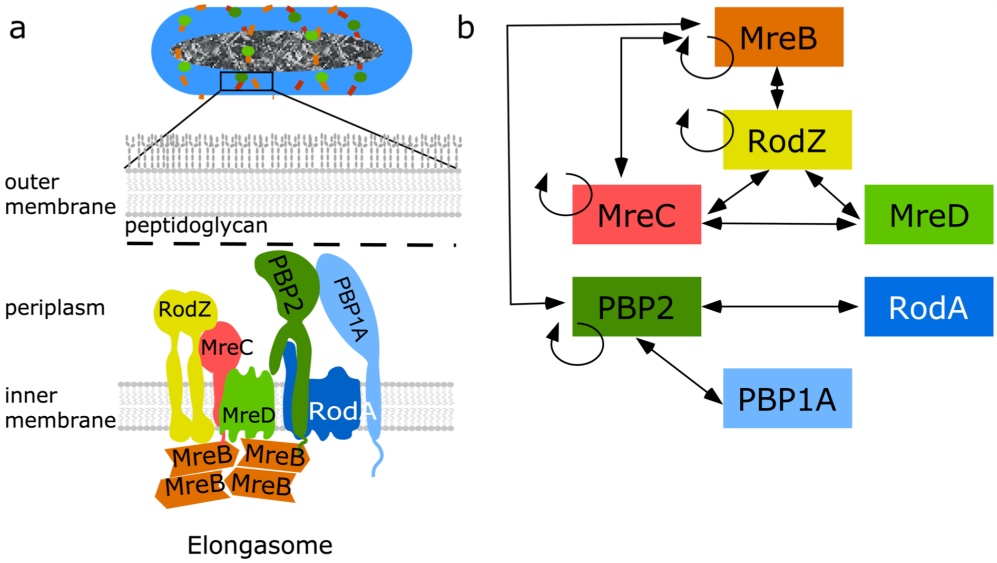

Figure 1. Core elongasome proteins and their interactions in *E. coli*. **a**. Schematic representation of the *E. coli* cell envelope and elongasome. MreB localizes in patches underneath the cytoplasmic membrane and recruits other elongasome proteins. The peptidoglycan layer is sandwiched by the cytoplasmic membrane and the outer membrane. **b**. Identified interactions between elongasome proteins from previous interaction studies (1-5). Double arrowed lines represent the interaction between different proteins. Circular arrows indicate self-interaction.

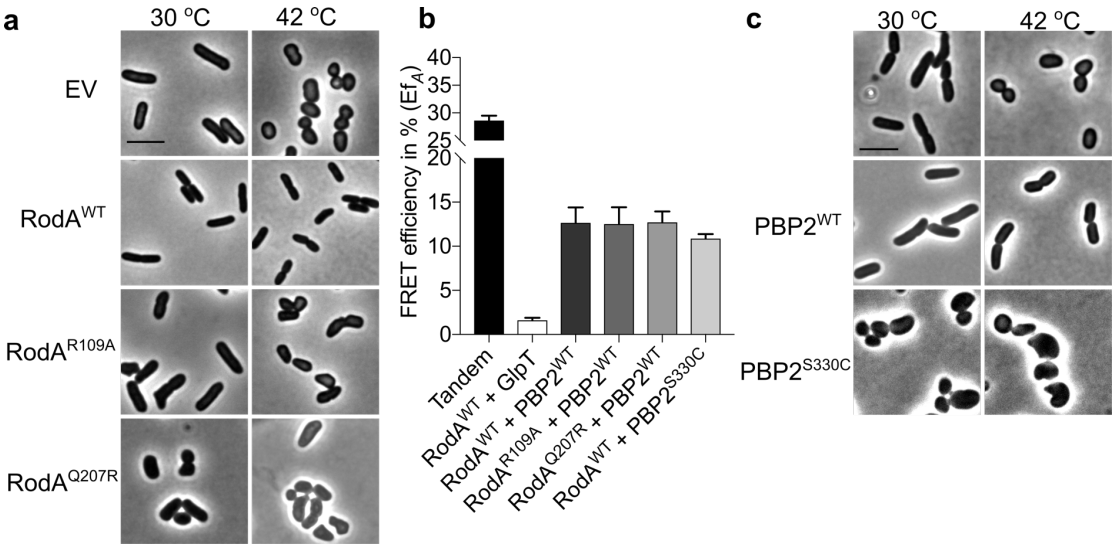

Figure 2. Activity of RodA and PBP2 are not required for their interaction. a, Phase contrast images of the complementation of RodA variants. RodA temperature sensitive strain LMC882 was transformed with plasmids expressing RodA variants and grown in LB medium at 30 °C (left panel) and 42 °C (right panel) for 2 mass doublings (with15 μM IPTG induction). EV, empty vector. **b**, Calculated acceptor FRET efficiencies (Ef_A) between PBP2 and RodA variants from spectral FRET measurements. RodA and its variants are fused with mCherry. PBP2 and its variants are fused with mKO. **c**. Phase contrast images of the complementation of PBP2 variants. The PBP2 temperature sensitive strain LMC582 was transformed with $PBP2^{WT}$ or $PBP2^{S330C}$, and grown in LB medium at 30 °C (left panel) and 42 °C (right panel) for 2 mass doublings (with 15 μM IPTG induction). Scale bar equals 5 μm. All the results in the figure are representative of at least three independent experiments.

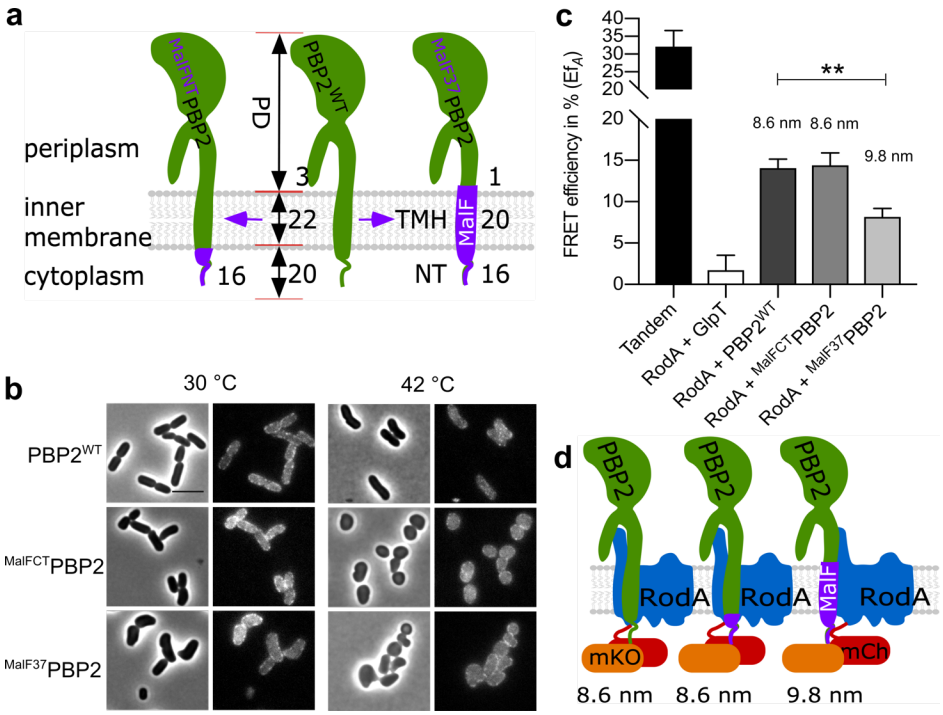

Figure 3. Functionality and interaction of PBP2 domain swap mutants. **a**. Schematic illustration of PBP2 domain-swap mutants. NT: N-terminus; TMH: transmembrane helix; PD: periplasmic domain; $PBP2^{WT}$: wild type PBP2; $^{MalFNT}PBP2$: the cytoplasmic N-terminus of PBP2 was replaced with the MalF cytoplasmic N-terminus; $^{MalF37}PBP2$: the NT and TMH domains of PBP2 were replaced with corresponding domains of MalF. Numbers indicate the residues involved in replacements in each domain of the proteins. **b**. Phase contrast and fluorescence images of the complementation of PBP2 mutants. The PBP2 temperature sensitive strain LMC582 was transformed with the PBP2 variants, and grown in LB medium at 30 °C (left panels) and 42 °C (right panels) for 2 mass doublings (with 15 μM IPTG induction). Scale bar equals 5 μm. **c**. Calculated acceptor FRET efficiencies (Ef_A) between PBP2 and RodA variants from spectral FRET measurements. RodA and its variants are fused with mCherry. PBP2 and its variants are fused with mKO. P value determined with Student's t-test (**: $p<0.001$). The numbers are apparent distances between the two proteins (fluorophores) and were calculated using the equation, $E = (1+(r/R_0)^6)^{-1}$, where r is the distance between the chromophores and R_0 (the Förster distance) is 6.4 nm for the mCh-mKO pair. **d**. Schematic illustration of the interaction between RodA and PBP2 variants. After replacement of the TMH domain of PBP2, by the TMH of MalF, the FRET efficiency is lower indicating that the distance between the FP fused TMHs of PBP2 and RodA has increased. However the interaction is not lost, indicating

that periplasmic domains are also involved in the interaction All results in the figure are representative of at least three independent experiments.

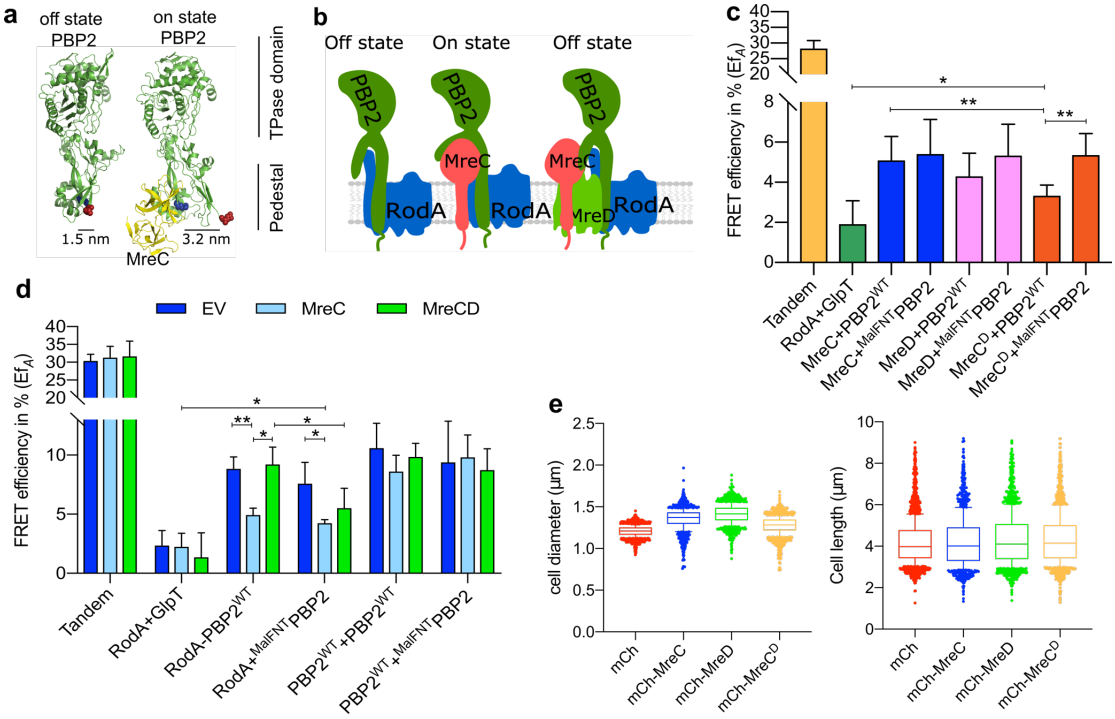

Figure 4. The balance of MreC and MreD affects the interaction between RodA and PBP2.

a. Crystal structures of *E. coli* PBP2 in different conformations (6) were modeled from *Helicobacter pylori* PBP2 structures (7) using Phyre2 (8). The structural information lacks the juxta-membrane, transmembrane helix and cytoplasmic regions of PBP2. MreC binds to PBP2 and was proposed to switch PBP2 from the "off state" to the "on state" (7). The distances between the two sphered residues, (blue for Glu157) and (red for Lys60) were calculated based on the structure of PBP2 in the different conformations. **b**. Schematic representation of PBP2 conformational changes caused by MreC. Left panels: PBP2 stays in the "off state" in the absence of MreC (the distance between the cytoplasmic terminus of RodA and PBP2 is small); middle panels: PBP2 switches to the "on state" after binding MreC (the distance between cytoplasmic terminus of RodA and PBP2 is larger), right panels: MreD suppresses the MreC-mediated conformational change of PBP2 and keeps PBP2 in the "off state". **c**. Calculated acceptor FRET efficiencies (Ef_A) between MreCD proteins and RodA variants from spectral FRET measurements. MreC: mCherry fused MreC; MreD: mCherry fused MreD; $MreC^D$: MreCD co-expressed from the same plasmid, and MreC is fused with mCherry while MreD is non-fused. PBP2 and its variants are fused with mKO. **d**. Calculated acceptor FRET efficiencies (Ef_A) between RodA and PBP2 variants from spectral FRET measurements in the three-plasmids FRET experiments. EV: a third empty vector; MreC: a third plasmid expressing non-

fused MreC; MreCD: a third plasmid expressing non-fused MreCD. **e**. Cell length and diameter changes after expressing MreC, MreD or MreCD together. LMC500 strain was transformed with each construct and grown in LB medium at 37 °C and induced with 15 μM IPTG for 2 mass doublings. Proteins were expressed from the pSAV057 derived plasmids (mKO: control; MreC: mKO fused MreC; MreD: mKO fused MreD; $MreC^{D}$: co-expression of MreC and MreD, MreC is fused with mKO while MreD is not fused. About 1000 cells were analyzed. P value determined with Student's t-test (*: $p<0.05$,; **: $p<0.01$:).

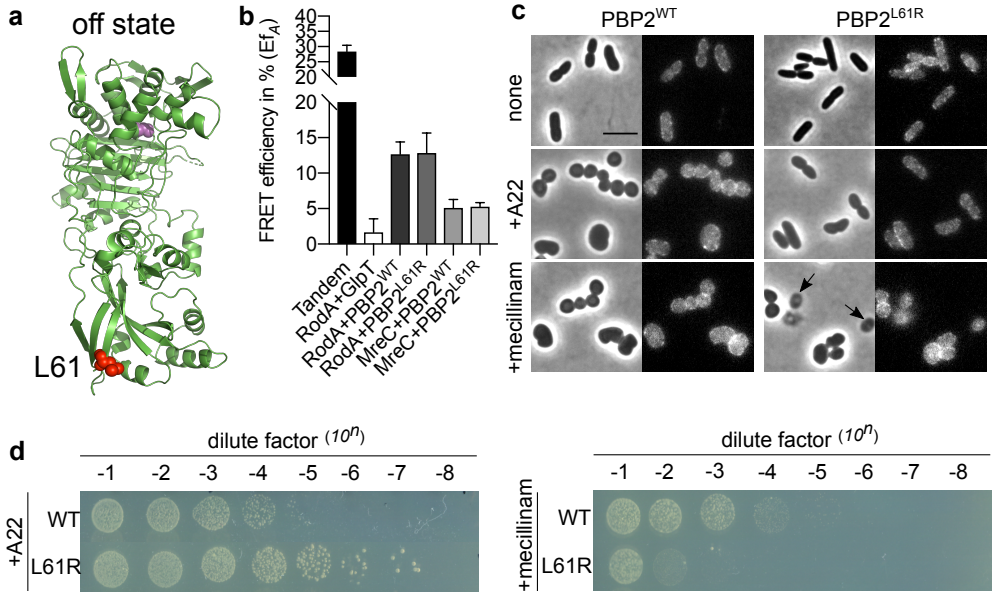

Figure 5. Hyperactive mutant PBP2^{L61R} is more sensitive to mecillinam. **a.** Modeled "off state" structure of *E. coli* PBP2 from *H. pylori* PBP2 using Phyre 2 (8). Structural information lacks on the juxta-membrane, transmembrane helix and cytoplasmic regions of PBP2. Residue Leu61 is colored in red and shown as spheres. Active site Ser330 is colored in pink and shown as spheres. **b**. Hyperactive mutant PBP2^{L61R} interacts similar like PBP2^{WT} with RodA and MreC. RodA and MreC were fused with mCherry, and PBP2^{WT} and PBP2^{L61R} were fused with mKO. **c**. Phase contrast and fluorescence images of cells expressing PBP2^{L61R} were less sensitive to A22 but hypersensitive to mecillinam in liquid culture. LMC500 strain expressing nothing, or PBP2^{WT}, or PBP2^{L61R} were grown in LB medium at 37 °C. IPTG induction (15 μM), and A22 treatment (10 mg·L^{-1}) or mecillinam treatment (2 mg·L^{-1}) were applied to each culture for 2 mass doublings. Arrows indicate cells that lysed after mecillinam treatment in the PBP2^{L61R} culture. Scale bar equals 5 μm. **d**. Spot assay to test the sensitivities of PBP2^{WT} and PBP2^{L61R} to A22 (10 mg·L^{-1}) and mecillinam (2 mg·L^{-1}).

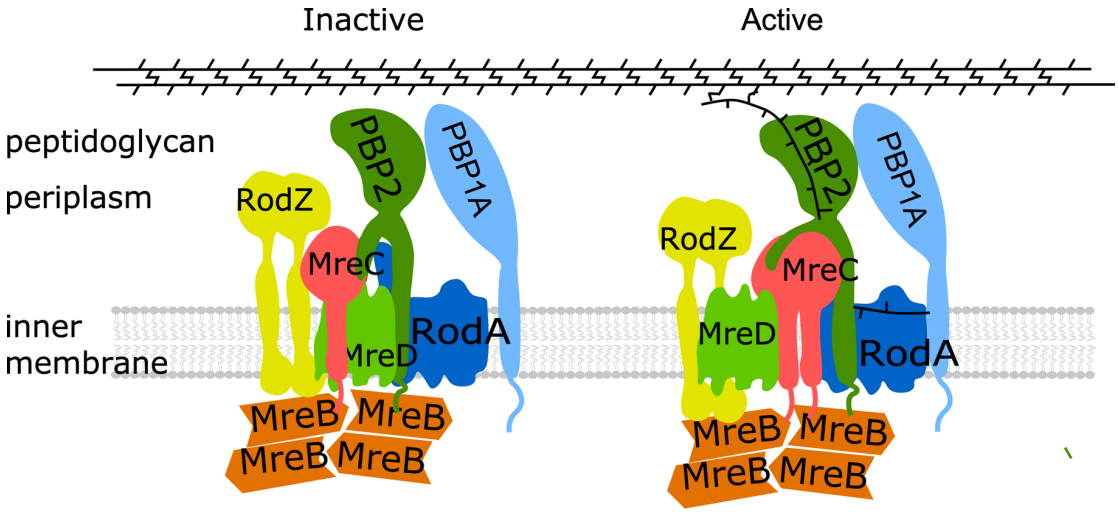

Figure 6. Model for regulation of elongasome and PG synthesis. RodA and PBP2 interact with each other and form a stable subcomplex. MreC and RodZ interact strongly with MreB filaments that likely link MreB to the PG synthesis proteins. MreC interacts with PBP2 that could stimulate and activate PBP2, while MreD, which interacts with both PBP2 and MreC, suppresses the activation of PBP2 by MreC, and keeps PG synthesis under control. The accumulation of MreC to the elongasome will finally abolish the inhibition of MreD and activate PBP2 by changing its conformation from the “off state” to the “on state”, and subsequently activate the elongasome and PG synthesis.

References:

1. Kruse T, Bork-Jensen J, Gerdes K. 2005. The morphogenetic MreBCD proteins of Escherichia coli form an essential membrane-bound complex. Mol Microbiol 55:78–89. https://doi.org/10.1111/j.1365-2958.2004.04367.x

2. Bendezú FO, Hale CA, Bernhardt TG, De Boer PAJ. 2009. RodZ (YfgA) is required for proper assembly of the MreB actin cytoskeleton and cell shape in E. coli. EMBO J 28:193–204. https://doi.org/10.1038/emboj.2008.264

3. Ikebe R, Kuwabara Y, Chikada T, Niki H, Shiomi D. 2018. The periplasmic disordered domain of RodZ promotes its self-interaction in Escherichia coli. Genes to Cells 23:307–317. https://doi.org/10.1111/gtc.12572

4. Banzhaf M, van den Berg van Saparoea B, Terrak M, Fraipont C, Egan A, Philippe J,

Zapun A, Breukink E, Nguyen-Distèche M, den Blaauwen T, Vollmer W. 2012. Cooperativity of peptidoglycan synthases active in bacterial cell elongation. Mol Microbiol 85:179–194. https://doi.org/10.1111/j.1365-2958.2012.08103.x

5. van der Ploeg R, Goudelis ST, den Blaauwen T. 2015. Validation of FRET assay for the screening of growth inhibitors of escherichia coli reveals elongasome assembly dynamics. Int J Mol Sci 16:17637–17654. https://doi.org/10.3390/ijms160817637
6. Rohs PDA, Buss J, Sim SI, Squyres GR, Srisuknimit V, Smith M, Cho H, Sjodt M, Kruse AC, Garner EC, Walker S, Kahne DE, Bernhardt TG. 2018. A central role for PBP2 in the activation of peptidoglycan polymerization by the bacterial cell elongation machinery. PLoS Genet 14:1–25. https://doi.org/10.1371/journal.pgen.1007726
7. Contreras-Martel C, Martins A, Ecobichon C, Trindade DM, Matteï P-J, Hicham S, Hardouin P, Ghachi M El, Boneca IG, Dessen A. 2017. Molecular architecture of the PBP2–MreC core bacterial cell wall synthesis complex. Nat Commun 8:776. https://doi.org/10.1038/s41467-017-00783-2
8. Kelley LA, Sternberg MJE. 2009. Protein structure prediction on the Web: a case study using the Phyre server. Nat Protoc 4:363. https://doi.org/10.1038/nprot.2009.2